# Conductance Spectroscopy of Majorana Zero Modes in Superconductor-Magnetic Insulator Nanowire Hybrid Systems

**Bhaskaran Muralidharan** (baskrons@gmail.com)
Indian Institute of Technology https://orcid.org/0000-0003-3541-5102
**Roshni Singh**
Indian Institute of Technology

**Article**

**Keywords:**

**Posted Date:** May 9th, 2022

**DOI:** https://doi.org/10.21203/rs.3.rs-1566363/v1

# Conductance Spectroscopy of Majorana Zero Modes in Superconductor-Magnetic Insulator Nanowire Hybrid Systems

Roshni Singh[1] and Bhaskaran Muralidharan[2]

[1] *Department of Physics, Indian Institute of Technology Bombay, Powai, Mumbai-400076, India*
[2] *Department of Electrical Engineering, Indian Institute of Technology Bombay, Powai, Mumbai-400076, India**

(Dated: April 17, 2022)

There has been a recent interest in superconductor-magnetic insulator hybrid Rashba nanowire setups for potentially hosting Majorana zero modes at smaller external Zeeman fields. Using the Keldysh non-equilibrium Green's function technique, we develop a detailed quantum transport approach that accounts for the complex interplay between the quasiparticle dynamics in the superconductor-magnetic insulator bilayer structure, and the transport processes through the semiconducting Rashba nanowire. We provide a detailed analysis of three terminal setups to probe the local and non-local conductance spectra in both the pristine as well as the disordered nanowire setups. We uncover the Majorana conductance quantization scaling with the bilayer coupling and the signatures of the gap closing and reopening followed by the emergence of near-zero energy states, which can be attributed to topological zero modes in the clean limit. However, in the presence of a smoothly varying disorder potential, trivial Andreev bound states may form with signatures reminiscent of topological zero modes in the form of a premature gap closure in the conductance spectra. Our results therefore provide transport-based analysis of the operating regimes that support the formation of Majorana modes in these hybrid systems of current interest, while investigating the effect of disorder on experimentally relevant device structures.

## I. INTRODUCTION

Rashba nanowire-superconductor hybrid systems [1–7] are the front-running platforms for detecting and manipulating Majorana zero modes (MZMs) [8–12]. The quantized zero-bias conductance peak (ZBCP), observed in two terminal setups featuring the normal metal - topological superconductor (N-TS) link, once considered to be a definitive signature of Majorana zero modes [13–18], has become a controversial issue. Quasi-MZMs [19–22], which are near-zero energy trivial Andreev bound states (ABS) mimic most of the MZM signatures. As a result, recent efforts [23–30] have focused on distinguishing between trivial and topological zero-energy modes. Recent proposals have considered measuring all the elements of the conductance matrix, particularly focusing on non-local transport measurements using three-terminal normal-topological superconductor-normal (N-TS-N) setups to identify the bulk-gap closing and reopening, which separates the trivial and topological regimes [31–36]. Non-local conductance signatures could supplement the local conductance measurements in identifying MZM signatures by detecting non-trivial correlations particularly in the presence of disorder.

With the aforementioned on one hand, the basic Rashba wire setup has further drawbacks which includes the requirement of large magnetic fields that could potentially destroy superconductivity [37–40] apart from the practicalities of precise magnetic field alignment [41]. Recently, efforts are being made towards realizing topological superconductivity with zero external magnetic fields by using proximity effects from magnetic insulators (MI) [42–52]. Recent experimental [43] and theoretical works [44–48, 51] featuring this setup indicate that at very low external magnetic fields, or even zero external magnetic fields, a topological MZM phase can emerge. The object of this paper is hence to provide an in-depth analysis of the transport signatures of MZMs in these structures, particularly focusing on the local and non-local conductance spectra in both pristine and disordered nanowires.

Using the Keldysh non-equilibrium Green's function (NEGF) technique, we develop a detailed quantum transport approach that accounts for the complex interplay between the quasiparticle dynamics in the superconductor-magnetic insulator (SC-MI) bilayer structure, and the transport processes through the semiconducting Rashba nanowire. Using this, we provide a detailed analysis of three terminal setups to probe the local and non-local conductance spectra in both the pristine as well as the disordered cases. We uncover the conductance quantization scaling with the bilayer coupling and the signatures of the gap closing followed by the emergence of near-zero energy states, which can be attributed to the zero modes in the clean nanowire. However, in the presence of a smoothly varying disorder potential, trivial Andreev bound states may form with signatures reminiscent of topological zero modes.

## II. RESULTS AND DISCUSSIONS

We consider semiconductor nanowires (SM) with Rashba-spin-orbit coupling with epitaxial layers of su-

* bm@ee.iitb.ac.in

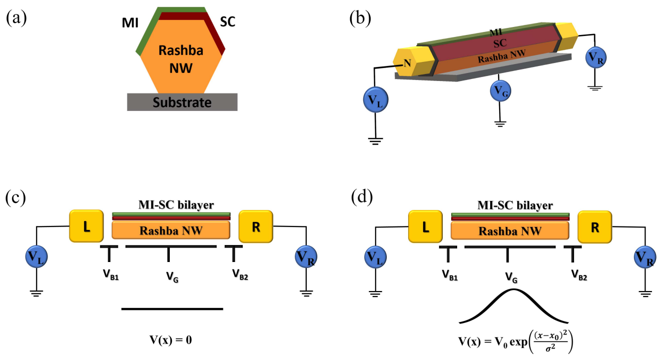


FIG. 1. Device schematics. (a) Cross section of Rashba nanowire epitaxially epitaxially coated with SC and MI, showing overlapping superconducting and magnetic-insulator layers. (b) A 3-D schematic of the device setup with the nanowire connected to two normal contacts via tunnel barriers, and a gate to control chemical potential, $\mu$. (c) and (d) Effective 1D models used for computation, treating MI-SC as a stacked bilayer, with the homogeneous and inhomogeneous chemical potential profiles shown below.

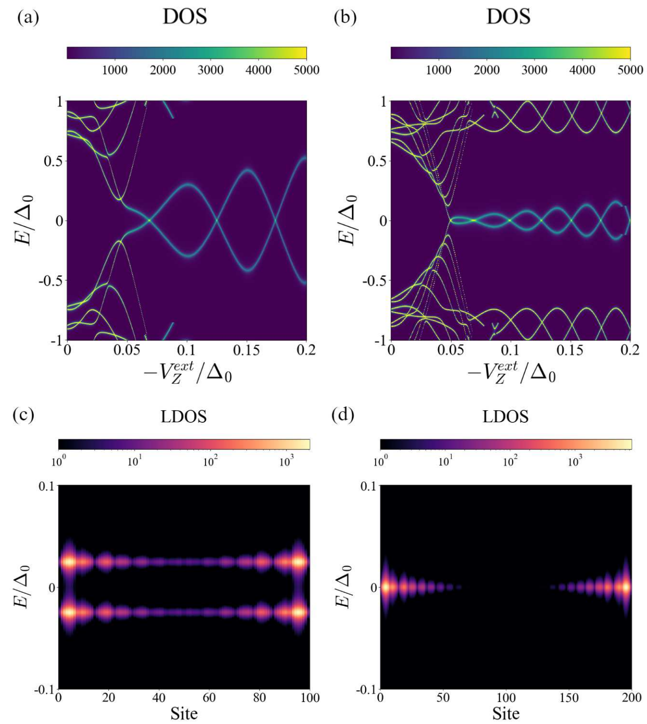


FIG. 2. MZMs in the structure. (a), (b) DOS of the device region for nanowire lengths (a) 2.25$\mu m$, and (b) 4.5$\mu m$. The low energy DOS shows the gap closing, followed by the emergence of a state near zero energy. The splitting of this low energy state is greater for shorter nanowires than longer nanowires. (c) and (d) LDOS profiles at $V_Z^{ext} = 0.1\Delta_0$ which clearly show the localization of the zero energy states at the ends of the nanowire, consistent with the appearance of MZMs. The longer (length 4.5$\mu m$) nanowire (d) shows a greater degree of localization than the shorter (length 2.25$\mu m$) nanowire (c)

perconductors (SC) (usually Al/Pb) and magnetic insulators (MI) (usually EuS), as depicted in Fig. 1(a). We then consider the device geometry where the MI and SC are in contact with the SM individually and overlap with each other, and connected to metallic leads as depicted in Fig. 1(b). The isolated Rashba nanowire is described by the following Hamiltonian:

$$H_{SM} = V_Z^{SM}\hat{\sigma}_x + (\frac{\hbar^2 k^2}{2m^*} - \mu + \alpha_R k\hat{\sigma}_y)\hat{\tau}_z, \qquad (1)$$

Where $V_Z^{SM}$ is the Zeeman Hamiltonian in the SM, $\mu$ is the electrochemical potential, $\alpha_R$ is the strength of the Rashba spin-orbit coupling, $m^*$ is the effective mass of the electron and $\hat{\sigma}_i, \hat{\tau}_i$, are the Pauli matrices in the spin and the particle-hole space, respectively.

The effects of the SC-MI bilayer are accounted for as a self-energy term in the Green's function for the nanowire and the effect of the direct coupling of the MI to the nanowire is taken to be an effective Zeeman field in the wire. We also use the self-consistent value of the superconducting gap, $\Delta$, calculated from the bare superconducting gap $\Delta_0$ of the parent superconductor in the presence of the Zeeman field and scattering processes. The process of obtaining this is involved and has been described in the supplementary material. We use $\Delta_0 = 0.23$ meV, $m^* = 0.015m_e$, where $m_e$ is the electron rest mass, for all our simulations.

In order to model the system to simulate transport measurements, we reduce the hexagonal nanowire to a quasi one-dimensional system [48] as shown in Fig. 1 (c) and (d). An external Zeeman field is applied which is anti-parallel to the magnetization in the MI. It reduces the Zeeman term in the Hamiltonian of the SC, but increases the Zeeman field in the normal metal. We parameterize the Zeeman fields in the SC and the SM in terms of the field directly induced in the SC due to the MI ($V_0^{SC}$), and the coupling strengths of the SC and SM nanowire to the external magnetic field, $(g_{SC}, g_{SM})$ as follows:

$$\begin{aligned} V_Z^{SC} &= V_0^{SC} + g_{SC}V_{ext}^Z \\ V_Z^{SM} &= g_{SM}V_{ext}^Z. \end{aligned} \qquad (2)$$

We use $g_{SC} = 2, g_{SM} = -15$ for our calculations, closely following the setup in [48], used for equilibrium calculations.

We first present the numerical results for the pristine nanowire, in the absence of an inhomogeneous potential. The low energy density of states (DOS) shown in Figs. 2 (a) and (b) illustrates the lowest ABS which form a near-zero energy oscillating mode after the topological transition, which is marked by the bulk gap closing and reopening. The bulk gap closing and reopening is more prominent in the longer nanowire than the shorter one, since there are more sub-gap states. As the length of the nanowire increases, the oscillations around zero-energy are exponentially suppressed.

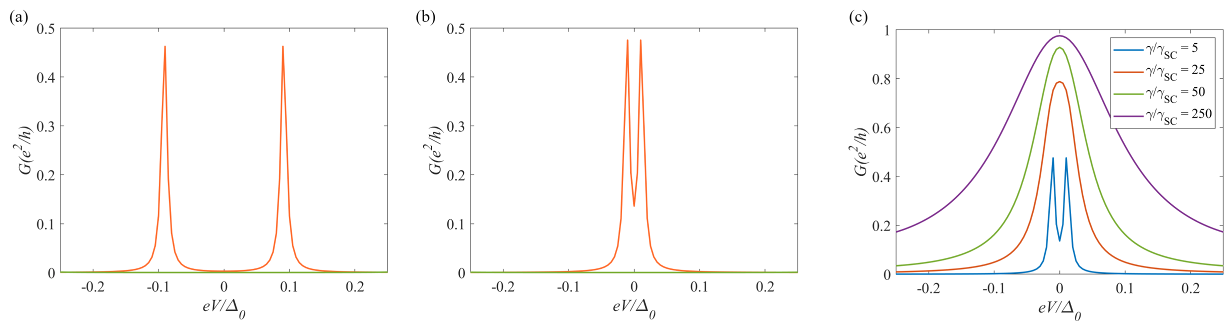


FIG. 3. Scaling of conductance quantization with bilayer coupling. (a) and (b) Low bias differential conductance plots for nanowire length (c) $4.5\mu m$, and (d)$2.25\mu m$). The topological region ($V_Z^{ext} = 0.07\Delta_0$) (orange) and trivial region ($V_Z^{ext} = 0.005\Delta_0$) (green). The topological regime shows clear conductance peaks absent in the trivial regime, though not quantized. The splitting of the zero bias peak can be seen for the shorter nanowire, consistent with Fig. 2.(c) Shows that as the coupling to the normal contacts, $\gamma$, is increased, so that it becomes much larger than the coupling, $\gamma_{SC}$, between the nanowire and the SC-MI bilayer, the peak asymptotically reaches the expected quantized value.

The local density of states (LDOS) corresponding to these nanowires shows that the zero energy state is well localised at both ends, and more prominently so in the longer nanowire. The LDOS plots also show a greater splitting in energy around the zero energy for the shorter nanowire than the longer nanowire. While on closer inspection, the longer nanowire also shows some splitting, in reasonable experimental measurements we expect to see a single broadened peak. These observations are due to the hybridization of the MZMs when they overlap in finite nanowires, resulting in a splitting of the zero mode [53]. The hybridization of the MZMs through the nanowire is suppressed with increasing length [54–56], which is consistent with our observations.

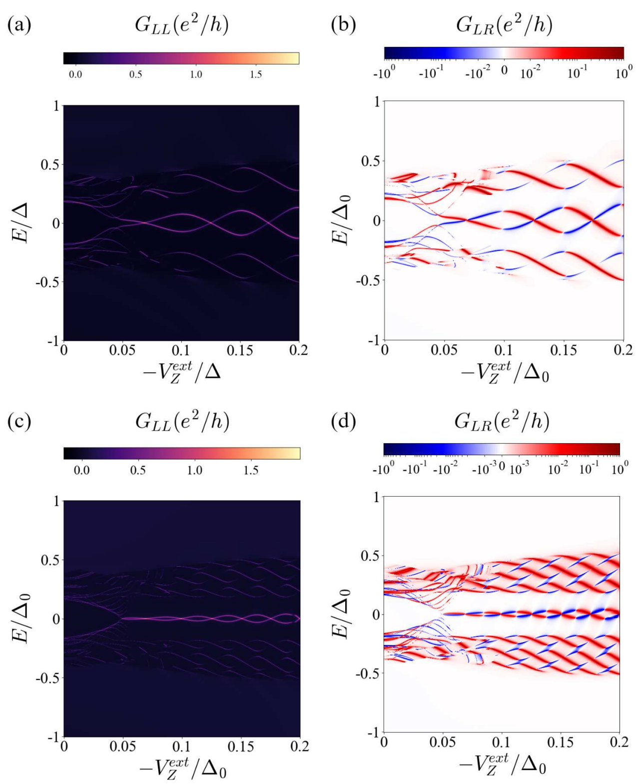


FIG. 4. Conductance spectra for the clean nanowire. (a) Local and (b) non-local conductance signatures for a nanowire of length 2.25 $\mu m$, with a potential profile as shown in Fig. 1(c). (c) Local and (d) non-local conductance spectra for a nanowire of length 4.5 $\mu m$, with a potential profile as shown in Fig. 1(c). Both the local and the non-local conductances show the bulk gap closing and reopening, which signals a topological transition, followed by the emergence of a near-zero energy state with a splitting that oscillates as a function of the externally applied magnetic field.

In Fig. 3, we plot the differential conductance for a clean nanowire with chemical potential $\mu = 0.125$meV and find a clear zero bias conductance peak in the topological regime, and no peak near zero energy in the topologically trivial regime. The peak is close to the quantized value of $\frac{e^2}{h}$ expected from an MZM in an N-S-N setup under symmetric biasing [54, 55], but is smaller. We attribute this observation to the level broadening in the presence of the proximitising SC-MI bilayer which effectively acts as an extra contact [57] and induces further broadening compared to a two-terminal N-TS-N device. This is also borne out by the fact that as the coupling to the metallic contacts becomes much stronger than the coupling to the bilayer, the ZBCP asymptotically reaches the quantized value, since the broadening due to the effective MI-SC bilayer becomes negligible in comparison to the broadening induced by the metallic contacts. It should also be noted that the exactness of the quantization would also depend on the external magnetic field because the Majorana overlap energy oscillates with the externally applied magnetic field. As the overlap energy of the MZMs at the ends of the nanowire varies, the peak value of the ZBCP also changes [58]. This figure clearly elucidates the effect of introducing the bilayer on the actual conductance quantization of MZMs in the setup.

Both the local and non-local conductances spectra for the pristine nanowire are shown in Fig. 4, which exhibit similar features, that is, the bulk gap closing and reopening followed by the emergence of Majorana oscillations

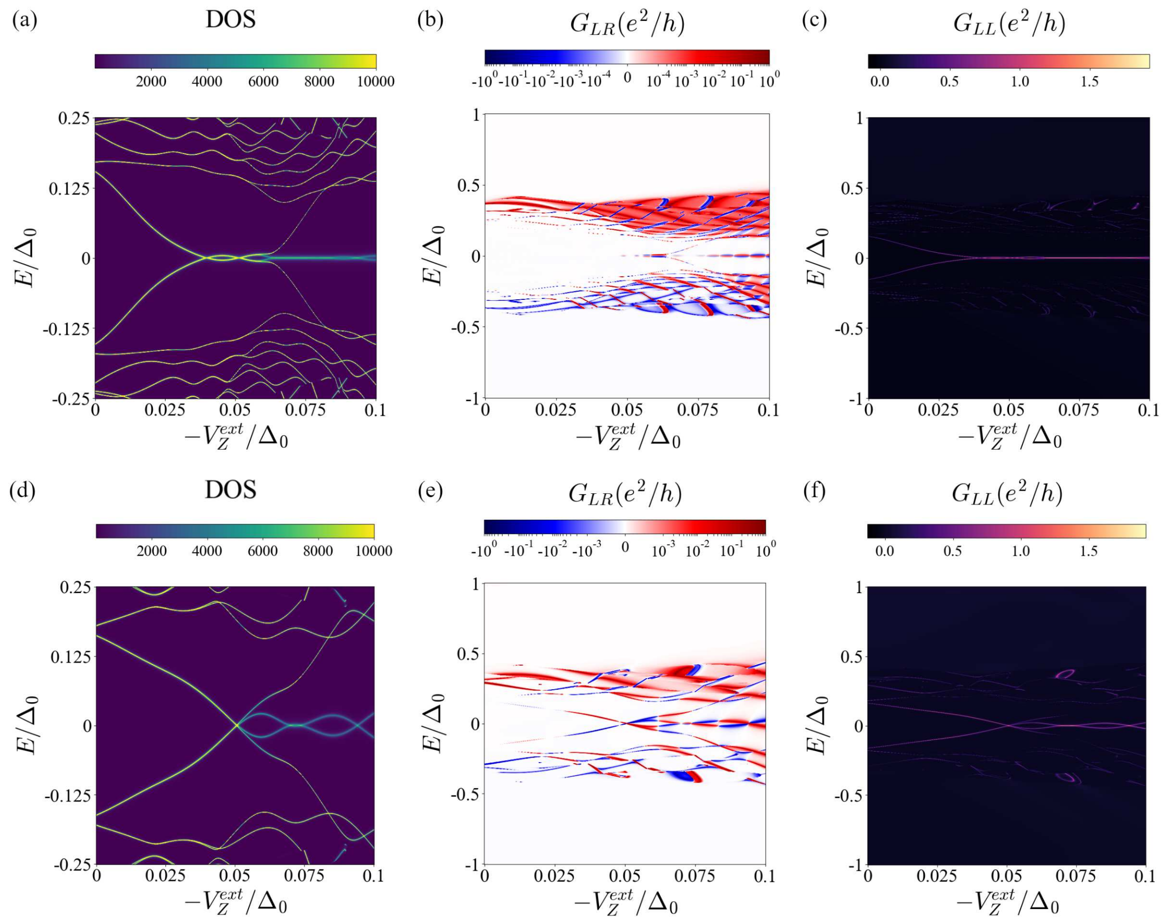


FIG. 5. Conductance spectra for the disordered nanowire. (a) Low Energy DOS (b) non-local and (c) local conductance spectra for a nanowire of length 4.5 $\mu m$, with a potential profile as shown in Fig. 1(d). (d) Low energy DOS, (e) the non-local and (f) the local conductance conductance spectra for a nanowire of length 2.25 $\mu m$, with a potential profile as shown in Fig. 1(d). For the long nanowire, we see premature emergence of a quasi-MZMs before the bulk gap closing and reopening.

around zero energy. Since the zero modes appear after the closure of the bulk gap, we can conclude that they are not quasi-MZMs, but may indeed be topological MZMs [59]. We also note that a finite low-bias non-local conductance only emerges after the topological transition. The low bias non-local conductance is rectifying in nature [31] and switches sign as the the voltage polarity is reversed. At the turning points, the non-local conductance vanishes.

For a single ABS level in the sub-gap region, there is a correspondence between the non-local conductance and the BCS charges of the bound state at the leads [60]. We can see that the BCS charge and the energy splitting oscillate out of phase. The vanishing of the non-local conductance at the turning points is a signature expected from hybridized MZMs, which should be chargeless at turning points. The local conductance is almost quantized at $\frac{2e^2}{h}$ where the Majorana splitting goes to zero. The deviation from the precise quantization value may be attributed to contact broadening, and due to the fact that we have three contacts in our system, as elaborated previously. At the points where the Majorana overlap energy becomes significant, the value of the local conductance drops further.

In presence of a smoothly-varying potential barrier, the formation of quasi-MZMs is expected [61–67]. They characteristically appear in the topologically trivial regime before the closure of the bulk gap, mimicking many signatures originally considered as 'smoking gun signatures' for MZMs including oscillations with the externally applied magnetic field, and with the associated local conductance quantized at values close to $\frac{2e^2}{h}$. It is expected that systems which show quasi-MZMs, will also exhibit true MZMs in the topological phase on increasing the external Zeeman field. For such a disordered case, for the longer nanowire, as shown in Fig. 5(a),(b) and (c), in the DOS, we find signatures characteristic of a quasi-MZM state, followed by a gap reopening signature and the emergence of a potential topological MZM. The local conductance in this case is quite deceptive since we see a premature gap closing and the bulk-gap reopening signature is extremely faint.

The quasi-MZM and the true MZM regions are quite difficult to distinguish. In the non-local conductance plot seen in Fig. 5(b), the bulk-gap reopening is seen more prominently. The non-local conductance shows signatures of both the quasi-MZM and the topological MZM states, which can be distinguished by their position with respect to the reopening of the bulk gap [61]. For the shorter nanowire, as seen in Figs. 5 (d),(e) and (f), the local and the non-local conductance spectra both show the gap closing and reopening followed by the emergence of MZMs, which oscillate in energy as the Zeeman field is increased. At the points where the splitting is zero, the local conductance is quantized at values very close to $\frac{2e^2}{h}$. We do not find any signatures of quasi-MZM states in this device. An interesting point to note is that the local conductance exhibits signs of negative differential conductance. It is also worth noting that especially for longer nanowires, neither the local nor the non-local conductance alone has the entire information regarding the channel DOS, that arises from its eigenspectrum.

The MZMs are protected by a clear topological gap both for the pristine nanowire and for the nanowire with a smoothly varying background potential. The local conductance fails to probe the bulk states for sufficiently long nanowires. Before one lays claim to having observed topological MZMs, it is necessary to measure the entire conductance matrix to probe a device and investigate whether the zero bias peaks at both the contacts or on both the sides are correlated and emerging after the bulk gap closing and reopening,

To conclude, using the NEGF technique, we developed a detailed quantum transport approach that accounts for the complex interplay between the quasiparticle dynamics in the SC-MI bilayer structure, and the transport processes through the semiconducting Rashba nanowire. We provided a detailed analysis of three terminal setups to probe the local and non-local conductance spectra in both the pristine as well as the disordered limits. We uncovered the conductance quantization scaling with the bilayer coupling and the signatures of the gap closing followed by the emergence of near-zero energy states, which can be attributed to the topological zero modes in the clean nanowire limit. However, in the presence of a smoothly varying potential, trivial Andreev bound states may form with signatures reminiscent of topological zero modes in the form of a premature gap closure in the conductance spectra. Our results therefore provide transport-based analysis of the operating regimes that support the formation of MZMs in these hybrid systems of current interest, while considering experimentally relevant device structures with realistic disordered potentials accounting for shallow tunnel barriers which may be formed inside the hybrid nanowire structure. Having set the stage for understanding device modeling in these emerging structures, the technique can also be easily extended to account for other experimental device designs and also the inclusion of scattering effects [54, 68] inside the nanowire channel.

## III. METHODS

We discretize the Hamiltonian of the system (2) on a 1D lattice with N sites, and write the Green's function in the Nambu spinor basis [69] $(\psi_\uparrow, \psi_\downarrow, -\psi_\uparrow^\dagger, \psi_\downarrow^\dagger)^T$. The Hamiltonian for the Rashba nanowire and the self-energies corresponding to the metallic contacts and the SC-MI bilayer, are then used obtain the retarded Green's function for the hybrid device which is used for our transport calculations,

$$G^R = \left[(E + i\eta)\mathbb{I} - H_{SM} - \Sigma_L - \Sigma_R - \Sigma'\right]^{-1}, \qquad (3)$$

where $\eta$ is an infinitesimal positive damping parameter introduced for numerical stability, and $\mathbb{I}$ is the identity matrix of the dimension of the Hamiltonian matrix in Nambu space. In the wide-band approximation [54–56], the self energies for the metallic contacts, $\Sigma_{L(R)}$, are written in their eigenbasis and are hence diagonal, as detailed in the supplementary material. We use the Usadel equation, which is derived from a quasi-classical approximation to the Gorkov equations, to find the Green's function, and hence, the self-energy, $\Sigma^{'}$ for the SC-MI bilayer [48]. The effect of the proximity of the MI on the SC can be taken into account in the boundary conditions of the Usadel equation. The MI layer induces a uniform Zeeman field $V_Z^{SC}$ in the diffusive superconductor[70]. The Usadel equation is then solved with the self-consistent value of $\Delta$ to obtain the quasi-classical Green's function for the bilayer, $\check{g}$. The gap is induced in the bare Rashba nanowire by considering the proximity effect of the bilayer, which is taken into account using the self energy, $\Sigma^{'}$ which can be obtained from the semi-classical Green's function, $\check{g}$. The imaginary part of $\Sigma^{'}$ connects the electron and hole subspaces, thus, inducing a gap in the system.

We also take into account spin-orbit and spin-flip scattering in the SC, by adding a scattering self-energy term in the Usadel equation. The energy scales for the spin-orbit and spin-flip relaxation processes are characterised by $\Gamma_{so}, \Gamma_{sf}$ respectively. We take $\Gamma_{so} = \Gamma_{sf} = 0.4\Delta_0$ for our simulations unless stated otherwise. We also use the Usadel Equation to calculate the self-consistent value of the superconducting gap in the presence of an external magnetic field. For this, we solve the Usadel equation self-consistently with the superconducting gap equation along with a thermodynamic constraint as outlined in the supplementary material.

We use the retarded Green's function defined above to calculate the conductance matrix for this setup [54–56, 69]. As shown in Fig. 1, we apply voltages $V_{L(R)}$ to the left and right contacts and measure terminal currents $I_{L(R)}$. We use the Keldysh non-equilibrium Green's function formalism to evaluate the terminal currents [54–56, 69]. The terminal electronic current at the left contact [71] can be derived in the Landauer Büttiker form as:

$$I_L^{(e)} = -\frac{e}{h}\left\{\int dET_A^{(e)}(E)\left[f\left(E-eV_L\right)-f\left(E+eV_L\right)\right]\right.$$
$$+\int dET_{CAR}^{(e)}(E)\left[f\left(E-eV_L\right)-f\left(E+eV_R\right)\right]$$
$$\left.+\int dET_D^{(e)}(E)\left[f\left(E-eV_L\right)-f\left(E-eV_R\right)\right]\right\}+I', \tag{4}$$

where, $T_D^{(e)}(E)$, $T_A^{(e)}(E)$, and $T_{CAR}^{(e)}(E)$ represent the energy resolved transmission probabilities for the direct, Andreev and crossed-Andreev processes involving the left and right contacts for the electronic sector of the Nambu space and I' is the extra current due to the SC-MI bilayer acting as an effective contact, derived in the supplementary material.

Using the expressions for the terminal currents from above, the conductance matrix $[G]$ can be defined as:

$$[\mathrm{G}] = \begin{pmatrix} G_{LL} & G_{LR} \\ G_{RL} & G_{RR} \end{pmatrix} = \begin{pmatrix} \left.\frac{\partial I_L}{\partial V_L}\right|_{V_R=0} & \left.\frac{\partial I_L}{\partial V_R}\right|_{V_L=0} \\ \left.\frac{\partial I_R}{\partial V_L}\right|_{V_R=0} & \left.\frac{\partial I_R}{\partial V_R}\right|_{V_L=0} \end{pmatrix}, \tag{5}$$

The diagonal matrix elements represent the local conductance at the left and right contacts, and the off-diagonal components represent the non-local conductance.

The local conductance at the left contact can be derived by taking a partial derivative of the left terminal current ($I_L$), as given in (4), with the left contact voltage ($V_L$), and the right contact voltage ($V_R$) set to zero, and is given by : $G_{LL} = \left.\frac{\partial I_L}{\partial V_L}\right|_{V_R=0}$. Using this, we derive the following expression for the local conductance using the Landauer Büttiker form

$$G_{LL}(V)|_{T\to 0} \equiv \frac{e^2}{h}\left[T_A(E=eV)+T_A(E=-eV)+\right.$$
$$\left.T_{CAR}(E=eV)+T_D(E=eV)+G_{LL}^{'}(V)\right], \tag{6}$$

The term $G_{LL}^{'}(V)$ is due to currents flowing into the SC-MI bilayer[56].

The non-local conductance formula can similarly be derived by taking a partial derivative of the left terminal current ($I_L$), as given in (4), over the right terminal voltage ($V_R$), with the left terminal voltage ($V_L$) set to zero, such that, $G_{LR} = \left.\frac{\partial I_L}{\partial V_R}\right|_{V_L=0}$.

$$G_{LR}(V)|_{T\to 0} \equiv \frac{e^2}{h}\left[T_{CAR}(E=-eV)-T_D(E=eV)\right]. \tag{7}$$

Using the above, we have analysed the local and non-local conductances of the device in both the pristine and disordered setups.

## DATA AVAILABILITY

The data that support the plots within this paper and other findings of this study are available from the corresponding author upon reasonable request.

## CODE AVAILABILITY

The codes generated during the simulation study are available from the corresponding author upon reasonable request.

## ACKNOWLEDGEMENTS

The author BM acknowledges the Visvesvaraya Ph.D Scheme of the Ministry of Electronics and Information Technology (MEITY), Government of India, implemented by Digital India Corporation (formerly Media Lab Asia). The author BM also acknowledges the support by the Science and Engineering Research Board (SERB), Government of India, Grant No. STR/2019/000030, and the Ministry of Human Resource Development (MHRD), Government of India, Grant No. STARS/APR2019/NS/226/FS under the STARS scheme. MSF and DC acknowledge support from the ARC Centre of Excellence in Future Low-Energy Electronics Technologies (CE170100039).

## AUTHOR CONTRIBUTIONS

BM and RS conceived the idea of this project. RS performed all numerical simulations. Both the authors contributed in analyzing the results and writing the paper.

## COMPETING INTERESTS

The authors declare that there are no competing interests.

[1] J. Alicea, Phys. Rev. B **81**, 125318 (2010).

[2] J. D. Sau and S. Tewari, Phys. Rev. B **88**, 054503 (2013).

[3] T. D. Stanescu and S. Tewari, Journal of Physics: Condensed Matter **25**, 233201 (2013).
[4] R. M. Lutchyn, J. D. Sau, and S. Das Sarma, Phys. Rev. Lett. **105**, 077001 (2010).
[5] J. D. Sau, R. M. Lutchyn, S. Tewari, and S. Das Sarma, Phys. Rev. Lett. **104**, 040502 (2010).
[6] J.-H. Jiang and S. Wu, Journal of Physics: Condensed Matter **25**, 055701 (2013).
[7] F. Wilczek, Nature **486**, 195 (2012).
[8] A. Y. Kitaev, Physics-Uspekhi **44**, 131 (2001).
[9] S. D. Sarma, M. Freedman, and C. Nayak, npj Quantum Information **1**, 1 (2015), 1501.02813.
[10] D. Aasen, M. Hell, R. V. Mishmash, A. Higginbotham, J. Danon, M. Leijnse, T. S. Jespersen, J. A. Folk, C. M. Marcus, K. Flensberg, and J. Alicea, Phys. Rev. X **6**, 031016 (2016).
[11] T. E. O'Brien, P. Rożek, and A. R. Akhmerov, Phys. Rev. Lett. **120**, 220504 (2018).
[12] C. Nayak, S. H. Simon, A. Stern, M. Freedman, and S. Das Sarma, Rev. Mod. Phys. **80**, 1083 (2008).
[13] A. Das, Y. Ronen, Y. Most, Y. Oreg, M. Heiblum, and H. Shtrikman, Nature Physics **8**, 887 (2012).
[14] V. Mourik, K. Zuo, S. Frolov, S. Plissard, E. Bakkers, and L. Kouwenhoven, Science **336**, 1003 (2012).
[15] M. T. Deng, V. S., E. Hansen, J. Danon, M. Leijnse, K. Flensberg, J. Nygård, P. Krogstrup, and C. M. Marcus, Science **354**, 1557 (2016).
[16] A. D. K. Finck, D. J. Van Harlingen, P. K. Mohseni, K. Jung, and X. Li, Phys. Rev. Lett. **110**, 126406 (2013).
[17] F. Nichele, A. C. C. Drachmann, A. M. Whiticar, E. C. T. O'Farrell, H. J. Suominen, A. Fornieri, T. Wang, G. C. Gardner, C. Thomas, A. T. Hatke, P. Krogstrup, M. J. Manfra, K. Flensberg, and C. M. Marcus, Phys. Rev. Lett. **119**, 136803 (2017).
[18] S. M. Albrecht, A. P. Higginbotham, M. Madsen, F. Kuemmeth, T. S. Jespersen, J. Nygård, P. Krogstrup, and C. M. Marcus, Nature **531**, 206 (2016).
[19] Y.-H. Lai, J. D. Sau, and S. Das Sarma, Phys. Rev. B **100**, 045302 (2019).
[20] J. Liu, A. C. Potter, K. T. Law, and P. A. Lee, Phys. Rev. Lett. **109**, 267002 (2012).
[21] D. Bagrets and A. Altland, Phys. Rev. Lett. **109**, 227005 (2012).
[22] D. J. Clarke, Phys. Rev. B **96**, 201109 (2017).
[23] A. Vuik, B. Nijholt, A. R. Akhmerov, and M. Wimmer, SciPost Phys. **7**, 61 (2019).
[24] G. Kells, D. Meidan, and P. W. Brouwer, Phys. Rev. B **86**, 100503 (2012).
[25] C. Fleckenstein, F. Domínguez, N. Traverso Ziani, and B. Trauzettel, Phys. Rev. B **97**, 155425 (2018).
[26] C.-X. Liu, J. D. Sau, T. D. Stanescu, and S. Das Sarma, Phys. Rev. B **96**, 075161 (2017).
[27] A. M. Lobos and S. D. Sarma, New Journal of Physics **17**, 065010 (2015).
[28] J. Cayao, E. Prada, P. San-Jose, and R. Aguado, Phys. Rev. B **91**, 024514 (2015).
[29] P. San-Jose, J. Cayao, E. Prada, and R. Aguado, Scientific Reports **6**, 21427 (2016).
[30] O. A. Awoga, J. Cayao, and A. M. Black-Schaffer, Physical Review Letters **123**, 117001 (2019).
[31] T. O. Rosdahl, A. Vuik, M. Kjaergaard, and A. R. Akhmerov, Phys. Rev. B **97**, 045421 (2018).
[32] J. Gramich, A. Baumgartner, and C. Schönenberger, Phys. Rev. B **96**, 195418 (2017).
[33] B. M. Fregoso, A. M. Lobos, and S. Das Sarma, Phys. Rev. B **88**, 180507 (2013).
[34] J. Danon, A. B. Hellenes, E. B. Hansen, L. Casparis, A. P. Higginbotham, and K. Flensberg, Phys. Rev. Lett. **124**, 036801 (2020).
[35] G. C. Ménard, G. L. R. Anselmetti, E. A. Martinez, D. Puglia, F. K. Malinowski, J. S. Lee, S. Choi, M. Pendharkar, C. J. Palmstrøm, K. Flensberg, C. M. Marcus, L. Casparis, and A. P. Higginbotham, Phys. Rev. Lett. **124**, 036802 (2020).
[36] D. Puglia, E. A. Martinez, G. C. Ménard, A. Pöschl, S. Gronin, G. C. Gardner, R. Kallaher, M. J. Manfra, C. M. Marcus, A. P. Higginbotham, and L. Casparis, Phys. Rev. B **103**, 235201 (2021).
[37] V. L. Ginzburg and L. D. Landau, in *On superconductivity and superfluidity* (Springer, 2009) pp. 113–137.
[38] G. Sarma, Journal of Physics and Chemistry of Solids **24**, 1029 (1963).
[39] B. Chandrasekhar, Applied Physics Letters **1**, 7 (1962).
[40] A. M. Clogston, Physical Review Letters **9**, 266 (1962).
[41] T. Karzig, C. Knapp, R. M. Lutchyn, P. Bonderson, M. B. Hastings, C. Nayak, J. Alicea, K. Flensberg, S. Plugge, Y. Oreg, *et al.*, Physical Review B **95**, 235305 (2017).
[42] R. Mélin, F. S. Bergeret, and A. L. Yeyati, Phys. Rev. B **79**, 104518 (2009).
[43] S. Vaitiekėnas, Y. Liu, P. Krogstrup, and C. Marcus, arXiv preprint arXiv:2004.02226 (2020).
[44] B. D. Woods and T. D. Stanescu, arXiv preprint arXiv:2011.01933 (2020).
[45] A. Maiani, R. S. Souto, M. Leijnse, and K. Flensberg, Physical Review B **103**, 104508 (2021).
[46] C.-X. Liu, S. Schuwalow, Y. Liu, K. Vilkelis, A. Manesco, P. Krogstrup, and M. Wimmer, Physical Review B **104**, 014516 (2021).
[47] J. Langbehn, S. A. González, P. W. Brouwer, and F. von Oppen, Physical Review B **103**, 165301 (2021).
[48] A. Khindanov, J. Alicea, P. Lee, W. S. Cole, and A. E. Antipov, Physical Review B **103**, 134506 (2021).
[49] Y. Liu, S. Vaitiekenas, S. Martí-Sánchez, C. Koch, S. Hart, Z. Cui, T. Kanne, S. A. Khan, R. Tanta, S. Upadhyay, *et al.*, Nano letters **20**, 456 (2019).
[50] S. Manna, P. Wei, Y. Xie, K. T. Law, P. A. Lee, and J. S. Moodera, Proceedings of the National Academy of Sciences **117**, 8775 (2020).
[51] S. D. Escribano, E. Prada, Y. Oreg, and A. L. Yeyati, Physical Review B **104**, L041404 (2021).
[52] S. D. Escribano, A. Maiani, M. Leijnse, K. Flensberg, Y. Oreg, A. L. Yeyati, E. Prada, and R. S. Souto, arXiv preprint arXiv:2203.06644 (2022).
[53] S. D. Sarma, J. D. Sau, and T. D. Stanescu, Physical Review B **86**, 220506 (2012).
[54] C. Duse, P. Sriram, K. Gharavi, J. Baugh, and B. Muralidharan, Journal of Physics: Condensed Matter **33**, 365301 (2021).
[55] N. Leumer, M. Grifoni, B. Muralidharan, and M. Marganska, Phys. Rev. B **103**, 165432 (2021).
[56] A. Kejriwal and B. Muralidharan, arXiv preprint arXiv:2112.02235 (2021).
[57] S. Datta, *Quantum transport: atom to transistor* (Cambridge university press, 2005).
[58] Y.-H. Lai, S. D. Sarma, and J. D. Sau, arXiv preprint arXiv:2111.01178 (2021).

[59] D. Puglia, E. Martinez, G. Ménard, A. Pöschl, S. Gronin, G. Gardner, R. Kallaher, M. Manfra, C. Marcus, A. P. Higginbotham, *et al.*, Physical Review B **103**, 235201 (2021).
[60] J. Danon, A. B. Hellenes, E. B. Hansen, L. Casparis, A. P. Higginbotham, and K. Flensberg, Physical Review Letters **124**, 036801 (2020).
[61] R. Hess, H. F. Legg, D. Loss, and J. Klinovaja, Physical Review B **104**, 075405 (2021).
[62] G. Kells, D. Meidan, and P. Brouwer, Physical Review B **86**, 100503 (2012).
[63] E. Prada, P. San-Jose, and R. Aguado, Physical Review B **86**, 180503 (2012).
[64] C.-X. Liu, J. D. Sau, T. D. Stanescu, and S. D. Sarma, Physical Review B **96**, 075161 (2017).
[65] A. Vuik, D. Eeltink, A. R. Akhmerov, and M. Wimmer, New Journal of Physics **18**, 033013 (2016).
[66] T. Rosdahl, A. Vuik, M. Kjaergaard, and A. Akhmerov, Physical Review B **97**, 045421 (2018).
[67] C. Reeg, O. Dmytruk, D. Chevallier, D. Loss, and J. Klinovaja, Physical Review B **98**, 245407 (2018).
[68] A. Singha and B. Muralidharan, Journal of Applied Physics **124**, 144901 (2018).
[69] P. Sriram, S. S. Kalantre, K. Gharavi, J. Baugh, and B. Muralidharan, Phys. Rev. B **100**, 155431 (2019).
[70] A. Cottet, D. Huertas-Hernando, W. Belzig, and Y. V. Nazarov, Physical Review B **80**, 184511 (2009).
[71] S. Datta, *Electronic Transport in Mesoscopic Systems* (Cambridge University Press, 1997).

# Supplementary Files

This is a list of supplementary files associated with this preprint. Click to download.

- SupplementaryMINWPaper.pdf